Symmetry effects in reversible random sequential adsorption on a triangular lattice

Lj. Budinski-Petković
Faculty of Engineering, Trg D. Obradovića 6, Novi Sad 21000, Serbia and Montenegro

M. Petković
DMS group, Puškinova 9A, Novi Sad 21000, Serbia and Montenegro

Z. M. Jakšić and S. B. Vrhovac
Institute of Physics, P. O. Box 68, Zemun 11080, Belgrade, Serbia and Montenegro

(Received 1 March 2005; revised manuscript received 20 June 2005; published 17 October 2005)

Reversible random sequential adsorption of objects of various shapes on a two-dimensional triangular lattice is studied numerically by means of Monte Carlo simulations. The growth of the coverage $\rho(t)$ above the jamming limit to its steady-state value ρ_∞ is described by a pattern $\rho(t)=\rho_\infty-\Delta\rho E_\beta[-(t/\tau)^\beta]$, where E_β denotes the Mittag-Leffler function of order $\beta\in(0,1)$. The parameter τ is found to decay with the desorption probability P_- according to a power law $\tau=AP_-^{-\gamma}$. The exponent γ is the same for all shapes, $\gamma=1.29\pm0.01$, but the parameter A depends only on the order of symmetry axis of the shape. Finally, we present the possible relevance of the model to the compaction of granular objects of various shapes.

DOI: 10.1103/PhysRevE.72.046118 PACS number(s): 02.50.−r, 68.43.Mn, 05.10.Ln, 45.70.Cc

I. INTRODUCTION

A large variety of physical, chemical, and biological processes can be modeled by random sequential adsorption (RSA) on a lattice [1]. In this process particles are adsorbed, one at a time, at randomly chosen sites of a d-dimensional lattice, subject to constraints imposed by interaction with previously deposited particles. The adsorbed particles are permanently fixed at their spatial positions. The deposition process ceases when all unoccupied spaces are smaller than the size of an adsorbed particle. The system is then jammed in a nonequilibrium disordered state. For lattice models, the asymptotic approach of the density $\rho(t)$ to its jamming limit ρ_{jam} is known to be given by the exponential time dependence

$$\rho(t) \sim \rho_{jam} - \Delta\rho \exp(-t/\sigma), \tag{1}$$

where $\Delta\rho$ and σ are parameters that depend on the shape and orientational freedom of depositing objects [1].

The deposition of proteins and colloids from solution onto solid surfaces often involves alternating adsorption and desorption steps. The kinetics of reversible RSA is governed by the ratio of adsorption to desorption rate, $K=k_+/k_-$. For large values of K, there is a rapid approach to the density $\rho \simeq \rho_{jam}$, followed by a slow relaxation to a larger steady-state value ρ_∞.

In this paper we present the results of Monte Carlo simulations for the reversible RSA of extended objects on a triangular lattice. Simulations are performed for objects of various shapes. These shapes are made by self-avoiding walks on the triangular lattice. Such walks are shown in Table I. We concentrate here on the influence of shape on the kinetics of the adsorption-desorption processes. On a triangular lattice objects with a symmetry axis of first, second, third, and sixth order can be formed and we analyze the impact of the order of symmetry on the kinetics of the process.

Understanding the kinetics of irreversible and reversible RSA of shapes other than line segments on a planar lattice lacks rigorous results by analytical methods due to their intractability. Numerical simulations, as one of the primary tools for investigating these problems, suggest that the shape of the object does play a significant role in the processes of irreversible deposition. Numerical analyses for RSA on a triangular lattice [2] establish that the coverage $\rho(t)$ follows the exponential law (1) at large times for all the shapes in Table I with the rate σ dependent mostly on the order of symmetry of the shape.

Recently Khandkar *et al.* [3] have studied RSA of zero-area symmetric angled objects on a continuum substrate for the full range (0°–180°) of values of the arm angle ϕ. The asymptotic approach to the jamming limit ρ_{jam} was shown to follow the expected algebraic behavior, $\rho_{jam}-\rho(t)\sim t^\alpha$. The value of the exponent α exhibits a crossover near $\phi=0°$ or 180°, and is significantly lower in the case of the angled objects than in the case of needles. This confirms the crucial role of the geometrical character of the objects in RSA dynamics.

In some numerical studies of RSA a power-law dependence is observed even on a discrete lattice. Wang and Pandey [4] have studied the kinetics and jamming coverage in RSA of self-avoiding walk chains on a square lattice. They reported that the growth of the coverage $\rho(t)$ to its jamming limit can be described by a power law $\rho(t)\sim\rho_{jam}-c/t^\gamma$ with an effective exponent γ that depends on the chain length ℓ. Lee and Hong [5] obtained qualitatively the same long-time behavior of the coverage density in a lattice model of RSA of k-mers with diffusional relaxation. However, the exponent γ of the power law depends on the diffusion length and on the length of the line segments. To the best of our knowledge, there are no reports on the *reversible* RSA of extended objects of shapes other than line segments [6,7] on a *triangular* lattice.

TABLE I. (Color online) Parameters τ and β determined using Eq. (2) for various shapes on a triangular lattice and for two different values of P_-. The colors (online only) are associated with different orders n_s of the symmetry axis.

	shape	n_s	ℓ	$P_- = 0.0005$		$P_- = 0.001$	
				τ	β	τ	β
(1)		2	2	895	0.823	402	0.888
(2)		2		986	0.711	434	0.776
(3)		1	3	675	0.822	279	0.904
(4)		3		1500	0.785	630	0.825
(5)		2		1048	0.678	431	0.732
(6)		1		608	0.822	242	0.851
(7)		1		583	0.853	249	0.908
(8)		2		1198	0.676	473	0.731
(9)		1	4	609	0.824	246	0.864
(10)		1		764	0.810	307	0.862
(11)		2		943	0.793	390	0.855
(12)		1		597	0.859	238	0.900
(13)		1		582	0.852	249	0.907
(14)		2	5	985	0.684	413	0.730
(15)		2		922	0.683	368	0.732
(16)		3		833	0.774	346	0.822
(17)		6	6	1950	0.595	808	0.647
(18)		1		605	0.745	241	0.821
(19)		2		807	0.681	353	0.731
(20)		6		1550	0.567	670	0.645
(21)		1	7	596	0.727	240	0.811
(22)		1		421	0.731	190	0.825

Recently, there has been a renewed interest in the reversible RSA because of its successful application to compaction of granular materials. An adsorption-desorption model can reproduce qualitatively the slow density relaxation [8], memory effects [9,10], and other features of weakly vibrated granular materials. This model can be regarded as a simple picture of a horizontal slice or layer of a real granular material, perpendicular to the tapping force. We associate an adsorption event with the filling of a void within the layer of granular material, whereas a desorption event is associated with creation of a void. The ratio of desorption to adsorption rate ($1/K=k_-/k_+$) plays in the model a role similar to the intensity of vibration Γ in real experiments. In that sense our two-dimensional lattice-based model could be viewed as a model for the compaction of granular objects of various shapes. However, there is a lack of systematic experimental investigations on the compaction of nonspherical granular materials under vibrations. Only a few papers discuss the problem of anisotropic particles [11–15].

The paper is organized as follows. Section II describes the details of the simulations. We give the simulation results and discussions in Sec. III. Finally, Sec. IV contains some additional comments and final remarks.

II. DEFINITION OF THE MODEL AND THE SIMULATION METHOD

The depositing objects are formed by self-avoiding random walks which are generated on the trails of nonreversal random walks with self-avoiding constraints. For a small number of steps it is easy to find all the shapes that may show different behavior, which enables a systematic approach to this problem. We performed numerical simulations for all such shapes of length $\ell=1$, 2, and 3, covering two, three, and four lattice sites, respectively. On a triangular lattice shapes with a symmetry axis of first, second, third, and sixth order can be formed. The simulations are also performed for a few more objects of greater lengths, including one more object with a symmetry axis of third order and two objects with symmetry axis of sixth order. All these objects are shown in Table I.

The Monte Carlo simulations are performed on a triangular lattice of size $L=120$. Periodic boundary conditions are used in all directions and objects are not allowed to overlap.

In the simulations of adsorption-desorption processes the time is usually rescaled to the adsorption process, because the number of adsorption attempts per unit of time is the quantity controlled in the experiments. The kinetics of the process is governed by the ratio of desorption to adsorption rate, which in our model corresponds to the ratio of desorption to adsorption probability. At each Monte Carlo step adsorption is attempted with probability P_+ and desorption with probability P_-. In order to save computer time it is convenient to take the adsorption probability to be $P_+=1$, i.e., to try an adsorption at each Monte Carlo step. For each of these processes a lattice site is selected at random. In the case of adsorption, we try to place the object with the beginning at the selected site, i.e., we search whether all relevant sites are unoccupied. If so, the object is placed and the corresponding sites are denoted as occupied. On the other hand, if the attempted process is desorption and if the selected site is already occupied by a previously adsorbed object, the object is removed from the layer.

The time t is counted by the number of adsorption attempts and scaled by the total number of lattice sites L^2. The

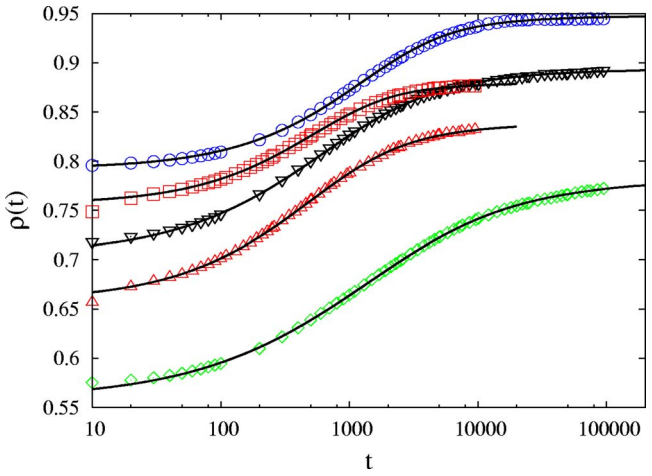

FIG. 1. (Color online) Temporal behavior of the density $\rho(t)$ for desorption probability $P_-=0.0005$ for various shapes from Table I: 4 (○), 9 (□), 17 (◇), 18 (△), and 19 (▽). The continuous curves are the Mittag-Leffler fits of Eq. (2), with the parameters given in Table I.

data are averaged over 100 independent runs for each shape and each desorption probability.

III. RESULTS AND DISCUSSION

The time behavior of the density $\rho(t)$ for various objects in Table I is illustrated in Fig. 1, where a relatively low value of P_- has been used ($P_-=0.0005$). We have observed that the relaxation of the system toward its equilibrium density ρ_∞ is a two-stage process: at very early times of the process, when the coverage is small, the adsorption process is dominant and the coverage grows rapidly in time; for large enough densities ($\rho > \rho_{jam}$) the compaction mechanism requires the rearrangement of the increasing number of particles [6,7] in order to open a hole large enough for the insertion of an additional particle, and the role of desorption is crucial.

Below we try to characterize the glassylike relaxation dynamics in our model quantitatively and make some quantitative predictions. We have tried to fit different functional forms to the simulation data in Fig. 1, looking in particular at the relaxation functions proposed in the experimental and numerical studies of disordered systems [16]. We have found that the commonly claimed stretched exponential relaxation does not hold for many objects, especially for those with symmetry axis of higher order ($n_s \geqslant 3$). Instead, the most suitable functional form for our data is a Mittag-Leffler function which is a natural generalization of the exponential function. The fitting function that we have used is

$$\rho(t) = \rho_\infty - \Delta\rho\, E_\beta(-(t/\tau)^\beta), \quad \Delta\rho = \rho_\infty - \rho_0, \tag{2}$$

where $\rho_\infty, \rho_0, \tau$, and β are the fitting parameters. E_β denotes the Mittag-Leffler function of order β. It is defined through the inverse Laplace transform:

$$E_\beta(-(t/\tau)^\beta) = \mathcal{L}[(u + \tau^{-\beta} u^{1-\beta})^{-1}], \tag{3}$$

from which the series expansion

$$E_\beta(-(t/\tau)^\beta) = \sum_{n=0}^{\infty} \frac{[-(t/\tau)^\beta]^n}{\Gamma(1+\beta n)} \tag{4}$$

can be deduced; in particular, $E_1(-t/\tau)=\exp(-t/\tau)$. The Mittag-Leffler function interpolates between the initial stretched exponential form

$$E_\beta(-(t/\tau)^\beta) \sim \exp\left(-\frac{1}{\Gamma(1+\beta)}(t/\tau)^\beta\right), \quad t \ll \tau, \tag{5}$$

and the long-time power-law behavior

$$E_\beta(-(t/\tau)^\beta) \sim \frac{1}{\Gamma(1-\beta)}(t/\tau)^{-\beta}, \quad t \gg \tau. \tag{6}$$

From Eqs. (2), (5), and (6), one obtains

$$\rho(t) \sim \begin{cases} \rho_\infty - \Delta\rho \exp\left(-\dfrac{1}{\Gamma(1+\beta)}(t/\tau)^\beta\right), & t \ll \tau, \quad (7) \\ \rho_\infty - \Delta\rho \dfrac{1}{\Gamma(1-\beta)}(t/\tau)^{-\beta}, & t \gg \tau. \quad (8) \end{cases}$$

The solid lines through the data in Fig. 1 are fits to Eq. (2). All fits have been performed for $\rho(t) \gtrsim \rho_{jam}$. As can be seen, the intermediate- to long-time behavior can be accurately fitted by the Mittag-Leffler function (2). The fitting parameters τ and β are given in Table I for two values of desorption probability: $P_-=0.0005$ and 0.001. The parameter ρ_∞ is the equilibrium value of $\rho(t)$ when $t \to \infty$, and $\rho_0 \approx \rho_{jam}$. Accurate estimates for the jamming coverages ρ_{jam} can be found in [2].

According to τ, all shapes from Table I can be divided into four groups. In particular, when $P_-=0.0005$ we distinguish (i) shapes with a symmetry axis of first order, $n_s=1$, with $\tau \leqslant 764$; (ii) shapes with a symmetry axis of second order, $n_s=2$, with $\tau \in [807–1198]$; (iii) shapes with a symmetry axis of third order, $n_s=3$, with $\tau \in [833–1500]$; and (iv) shapes with a symmetry axis of sixth order, $n_s=6$, with $\tau \geqslant 1550$. We notice that the time τ physically signals the crossover from a stretched exponential scaling (7) to a power-law behavior (8). If only $\beta \neq 1$, the relaxation has an algebraic decay. The shapes of higher order of symmetry n_s have higher values of τ. This means that the dynamics gets drastically slower when n_s increases. The crossover time τ is also sensitive to variations of desorption probability P_- and decreases with increasing P_- for the same type of shape. The data for k-mers (objects 1, 2, 5, 14, 15, and 19 in Table I) suggest that the parameter τ is almost independent of the size of the shape. However, the fitting parameter β depends both on the symmetry order and on the size of the object. The parameter β decreases with increasing size of the shape, which means that the evolution toward the steady-state density ρ_∞ takes place on a wider time scale.

In order to gain a better understanding of the symmetry effects, we investigated the dependence of the fitting parameters τ and β on desorption probability P_-, in detail. The data for τ and β vs P_- for various objects are plotted in Fig. 2. The increase of β with P_- is more pronounced for objects with higher order of symmetry axis. For large values of P_-, the parameter β reaches a value close to 1. Since

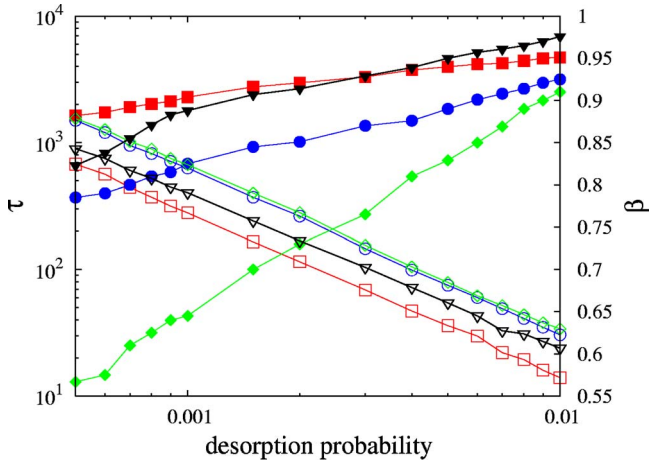

FIG. 2. (Color online) Parameters τ (empty symbols) and β (full symbols) of fit (2) vs desorption probability P_- for several shapes from Table I. Triangles, squares, circles, and diamonds correspond to shapes 1, 3, 4, and 20 in Table I, respectively.

$E_\beta(-(t/\tau)^\beta) \to \exp(-t/\tau)$ when $\beta \to 1$, the multistage relaxation feature disappears in the regime of strong desorption. It is remarkable that the parameter τ, for a given symmetry order, seems to be a simple power law of the desorption probability P_-:

$$\tau = A(P_-)^{-\gamma}, \tag{9}$$

with the same exponent $\gamma = 1.29 \pm 0.01$ for *all* shapes.

The dependence of the fitting parameters τ and β on the desorption probability P_- is shown in Fig. 3 for the reversible deposition of k-mers ($k=2-5$). The first observation is the collapse of the τ vs P_- curves. This means that the parameter A of the power law (9) can be considered as almost independent of the size of k-mers. As seen in Figs. 2 and 3, the parameter A depends only on the order of symmetry axis

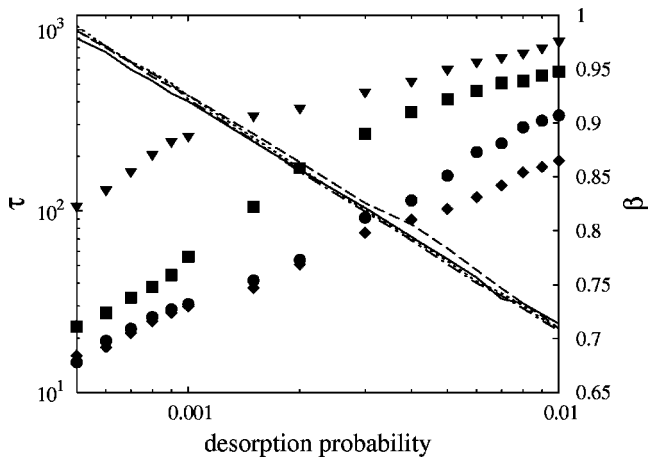

FIG. 3. Parameters τ (lines) and β (symbols) of fit (2) vs desorption probability P_- for k-mers ($k=2$, 3, 4, 5) on the triangular lattice. Triangles, squares, circles, and diamonds (or solid, dashed, dotted, and dot-dashed lines) correspond to $k=2$, 3, 4, 5, respectively.

of the shape. We have obtained that $A=0.038$, 0.058, 0.076, 0.083 for $n_s=1$, 2, 3, 6, respectively.

It is now useful to explore the possible reason for slowing down of the deposition dynamics with increasing order of symmetry of the shape. When a value of ρ_{jam} is reached, the rare desorption events are generally followed by immediate readsorption. The total number of particles is not changed by these *single*-particle events. However, when one badly sited object desorbs and two particles adsorb in the opened good locations, then the number of particles is increased by one. Likewise, if two well-sited objects desorb and a single object adsorbs in their stead, the number of particles is decreased by one. These *collective* events are responsible for the density growth above ρ_{jam}. The symmetry properties of the shapes have a significant influence on the filling of small isolated targets on the lattice. Indeed, there is only a restricted number of possible orientations in which an object can reach a previously opened location, provided the location is small enough. For a shape with symmetry axis of higher order there is a greater number of possible orientations for deposition into an isolated location and an enhanced probability for readsorption. Hence, the increase of the order of symmetry of the shape enhances the rate of single-particle readsorption. This extends the mean waiting time between consecutive two-particle events and causes a slowing down of the densification.

One striking feature of Fig. 3 is the fact that the fitting parameter β remarkably depends on the desorption probability P_- and on the object size. For small P_- and large objects the coverage fraction does not significantly change near the jamming limit ρ_{jam} and evolution takes place on a much wider time scale. This dynamical behavior is characterized by the small values of the fitting parameter β and can be associated with the competition of single- and two-particle events. Indeed, the single-particle events would drive the system to the jamming limit ρ_{jam} in a given time t. If t were small enough compared to the two-particle transition rate, the system would stay at $\rho(t) \gtrapprox \rho_{jam}$ until the two-particle events contributed to the dynamics. This results in the plateau in the time evolution of the coverage fraction. The length of this plateau is controlled by the desorption probability P_- and the object size, as these quantities determine the transition rates for two well-placed particles to one not well-placed particle and one not well-placed particle to two well-placed particles. This relaxation feature disappears in the regime of strong desorption when the fitting parameter $\beta \to 1$.

IV. CONCLUSION AND PERSPECTIVES

We have performed extensive simulations of reversible RSA using objects of different sizes and rotational symmetries on a triangular lattice. A systematic approach is made by examining a wide variety of object shapes. The large number of examined objects represents a good basis for testing various fitting functions and finding a universal functional type that describes the time coverage behavior $\rho(t)$ in the best way. We have fitted the time dependences of the coverage fraction above the jamming limit ρ_{jam} with the Mittag-Leffler

function (2). The simulation shows that the coverage kinetics strongly depends on the symmetry properties of the shapes. It was shown that the dynamical behavior is severely slowed down with the increase of the order of symmetry of the shape. We have also pointed out the importance of collective events for governing the time coverage behavior of shapes with different rotational symmetry.

Various experimental studies have underlined the fact that the dynamics of granular compaction is a complex problem. The first experiments [17] have shown that the density compaction under tapping follows an inverse logarithmic law with the tapping number $\rho(\infty)-\rho(t)\sim 1/\ln(t)$. More recently, Bideau and co-workers [15,18] showed that the compaction dynamics is consistent with the stretched exponential law

$$\rho(t) = \rho_\infty - (\rho_\infty - \rho_0)\exp[-(t/\tau)^\beta]. \tag{10}$$

Here ρ_0 is the initial packing fraction and ρ_∞ is the mean value of the packing fraction at the stationary state.

A number of different models have been proposed in order to identify the physical principles underlying granular compaction [19–22] without reaching a unique conclusion concerning the temporal behavior of the density change. However, when analyzing the previous experimental results [15,17,18], we found that the Mittag-Leffler behavior [Eq. (2)] describes excellently well the compaction dynamics in the whole temporal range. Our motivation arises from the fact that the Mittag-Leffler function is one of the most frequently used phenomenological fitting functions for non-Debye relaxation processes in many complex disordered systems such as metallic glasses, spin glass alloys, ferroelectric crystals, and dielectrics [23].

In Ref. [15], the authors analyzed the effect of the grain anisotropy on granular compaction under vertical tapping and reduced lateral confinement. They observed that the main relaxation features of granular compaction do not qualitatively depend on the grain shape. We produced a good fit of data from Ref. [15]. Our fits are shown in Fig. 4 for two tapping intensities Γ, and the fitting parameters are reported in Table II. It should be noted that Mittag-Leffler fit (2) of data from Ref. [15] gives very high correlation coefficients ($\gtrsim$0.99). Our simulation results for deposition of extended objects on a triangular lattice might indicate that the compaction law (2) is universal in the sense that it holds for any shape of granular object. Therefore, it needs to be clarified whether the Mittag-Leffler law is just a good fit to the experimental data or has a deeper meaning.

Let us conclude with two points that open possibilities for future work.

It is interesting to note that the fitting function (2) is a solution of the fractional kinetic equation [24]

$$\frac{d}{dt}\Delta\rho(t) = -\tau^{-\beta}\,{}_0D_t^{1-\beta}\Delta\rho(t), \quad 0<\beta<1, \tag{11}$$

where $\Delta\rho(t)=\rho_\infty-\rho(t)$. The operator ${}_0D_t^{1-\beta}$ is the Riemann-Liouville (RL) operator of fractional integration:

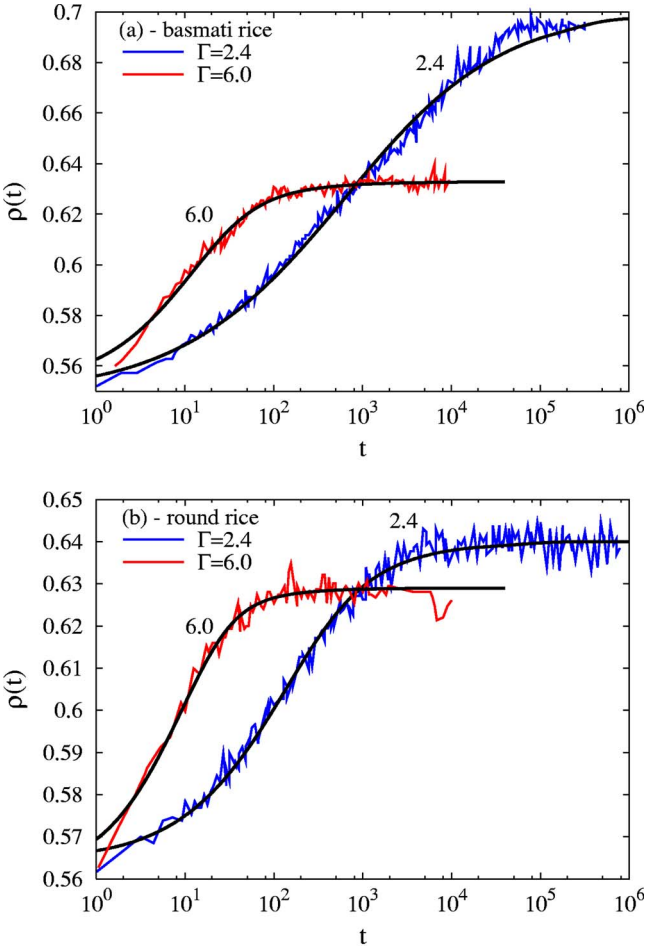

FIG. 4. (Color online) Experimental data from Ribière *et al.* [15] on temporal evolution of the mean volume fraction $\rho(t)$ of (a) basmati rice (long grains) and (b) round rice (short grains) for different tapping intensities $\Gamma=2.4$ and 6.0. The continuous superimposed lines are fits according to Eq. (2). The parameters of the fit are reported in Table II.

$${}_0D_t^{1-\beta}\Delta\rho(t) = \frac{1}{\Gamma(\beta-1)}\int_0^t (t-t')^{\beta-2}\Delta\rho(t')dt'. \tag{12}$$

The RL operator introduces a convolution integral into Eq. (11) with the power-law kernel $M(t)\propto t^{\beta-2}$. Therefore, the fractional kinetic equation (11) involves a slowly decaying memory, so the present density $\rho(t)$ of the system depends

TABLE II. Fitting parameters from Eq. (2) for the experimental data of Ribière *et al.* [15] on volume fraction relaxation $\rho(t)$ presented in Fig. 4. The anisotropic grains used are of two different shapes: long grains (basmati rice) and short grains (round rice).

	Γ	ρ_∞	ρ_0	τ	β
(Basmati rice)	2.4	0.702	0.548	1004.0	0.440
(Round rice)	2.4	0.640	0.564	181.0	0.665
(Basmati rice)	6.0	0.633	0.552	15.0	0.750
(Round rice)	6.0	0.629	0.560	10.5	0.838

strongly on its history $\rho(t')$, $t' < t$. This is in accordance with the fact that granular materials are intrinsically nonlocal. More detailed studies of this point are planned for the future in order to develop a fractional model of granular compaction that captures this relaxation dynamics.

As an open possibility for the future, we think that the two-dimensional model presented in this work can be generalized to mixtures of several kinds of objects [2]. This would allow us to study the compaction process in *polydisperse* granular systems under tapping [25].

ACKNOWLEDGMENTS

This research has been supported by the MNTRS under Projects No. 1895, No. 1469, and No. 1478.

[1] J. W. Evans, Rev. Mod. Phys. **65**, 1281 (1993).
[2] Lj. Budinski-Petković and U. Kozmidis-Luburić, Phys. Rev. E **56**, 6904 (1997).
[3] M. D. Khandkar, A. V. Limaye, and S. B. Ogale, Phys. Rev. Lett. **84**, 570 (2000).
[4] J.-S. Wang and R. B. Pandey, Phys. Rev. Lett. **77**, 1773 (1996).
[5] J. W. Lee and B. H. Hong, J. Chem. Phys. **119**, 533 (2003).
[6] R. S. Ghaskadvi and M. Dennin, Phys. Rev. E **61**, 1232 (2000).
[7] J. W. Lee, Physica A **331**, 531 (2004).
[8] J. Talbot, G. Tarjus, and P. Viot, Phys. Rev. E **61**, 5429 (2000).
[9] G. Tarjus and P. Viot, Phys. Rev. E **69**, 011307 (2004).
[10] Lj. Budinski-Petković and S. B. Vrhovac, Eur. Phys. J. E **16**, 89 (2005).
[11] F. X. Villarruel, B. E. Lauderdale, D. M. Mueth, and H. M. Jaeger, Phys. Rev. E **61**, 6914 (2000).
[12] G. Lumay and N. Vandewalle, Phys. Rev. E **70**, 051314 (2004).
[13] I. C. Rankenburg and R. J. Zieve, Phys. Rev. E **63**, 061303 (2001).
[14] P. Ribière, P. Richard, R. Delannay, and D. Bideau, Phys. Rev. E **71**, 011304 (2005).
[15] P. Ribière, P. Richard, D. Bideau, and R. Delannay, Eur. Phys. J. E **16**, 415 (2005).
[16] J. C. Phillips, Rep. Prog. Phys. **59**, 1133 (1996).
[17] J. B. Knight, C. G. Fandrich, C. N. Lau, H. M. Jaeger, and S. R. Nagel, Phys. Rev. E **51**, 3957 (1995).
[18] P. Philippe and D. Bideau, Europhys. Lett. **60**, 677 (2002).
[19] E. Caglioti, V. Loreto, H. J. Herrmann, and M. Nicodemi, Phys. Rev. Lett. **79**, 1575 (1997).
[20] M. Nicodemi, A. Coniglio, and H. J. Herrmann, Phys. Rev. E **55**, 3962 (1997).
[21] J. J. Brey and A. Prados, Phys. Rev. E **68**, 051302 (2003).
[22] J. Berg and A. Mehta, Phys. Rev. E **65**, 031305 (2002).
[23] R. Hilfer, J. Non-Cryst. Solids **305**, 122 (2002).
[24] R. K. Saxena, A. M. Mathai, and H. J. Haubold, Physica A **344**, 657 (2004).
[25] M. Wackenhut and H. Herrmann, Phys. Rev. E **68**, 041303 (2003).